

Grain boundary scars on spherical crystals

Thomas Einert¹, Peter Lipowsky¹*, Jörg Schilling¹, Mark Bowick² and Andreas R. Bausch¹*

¹Lehrstuhl für Biophysik E22, TU München, 85747 Garching, Germany

²Physics Department, Syracuse University, Syracuse NY 13244-1130, USA

* contributed equally to the work

Here we present an experimental system which allows the observation of grain boundary scars on the surface of a sphere. The introduction of fluorescently labeled particles enables us to determine the location and orientation of grain boundaries on the spherical surface. We find that the observed lengths of the scars are in good accordance with theoretical predictions and that the geometrical centers of the scars are nearly positioned at the vertices of an icosahedron.

When crystals form on curved surfaces it is known that new defect structures arise even at zero temperature. Dislocations form in the ground state of sufficiently large curved crystals because they lower the total elastic energy ¹⁻⁵. In the specific case of spherical crystals these dislocations may be viewed as screening the elastic strain of the isolated disclination defects required by the topology of the sphere. They are present, above a critical particle number of order 300, in the form of novel freely terminating high-angle grain boundaries dubbed scars ⁶.

Recently, these grain boundary scars were observed experimentally by bright field microscopy visualizations of Pickering emulsions. The images gathered and analyzed were of spherical caps subtending a solid angle ranging from 10 to 20% of the full 4π solid angle of the sphere. Since one expects a roughly icosahedral symmetry for the ground state it is actually sufficient to analyze 1/12 of the sphere to check the predictions of equilibrium statistical mechanics and we were able to confirm theoretical predictions for the length of the scars and also to analyze the dynamics of both particles and dislocation defects. In order, however, to properly check the global features of the crystalline ground state it is essential to observe the location and structure of several scars on the sphere – thus a bigger area has to be imaged. To achieve this, three dimensional (3D) information about all bead positions is necessary, and this can be obtained by laser scanning confocal microscopy (LSCM). For an automated triangulation it is necessary that the optical resolution and contrast of the image is sufficient for automatic bead detection.

In this paper we introduce an experimental system which allows the observation of the 3D positions of defects on spherical surfaces. An automated particle tracking and triangulation method has been established in order to determine the position of defects on the surface. The systems studied had a system size in the range of $R/a \sim 11$ to 14, and the scars observed had a length of about 5 dislocations. The position of the scars relative to each other was found to be near the vertices of an icosahedron, though deviations from the theoretically predicted ideal locations were often observed. This is attributed

to thermal fluctuations a local disturbances of the system. The results show that scars are generic structures inherent to the ground state of sufficiently large spherical crystals.

We have studied Pickering emulsions as model systems for curved 2D crystal ^{7, 8}. The Pickering emulsions studied here consist of water droplets in toluene solution stabilized by silica microspheres with a diameter of 1.5 μm ^{9, 10}. In order to prevent aggregation of the particles the microspheres were silanized with n-octyltrimethoxysilane (ABCR, Karlsruhe, Germany). The increased hydrophobicity was necessary to obtain stable and regular structures at the oil-water interface ¹¹. In order to minimize the water content of the final dispersion, fluorescently labeled silica particles (Sicastar Green F, Micromod, Rostock, Germany) were repeatedly dried and redispersed, first in ethanol, then in acetone, before they were transferred to anhydrous toluene. 300 μl silane was added to the final volume of 5 ml together with a catalyser (25 μl butylamine). After incubation in an ultrasonic bath for one hour under continuous stirring, the particles were repeatedly centrifuged and washed with acetone and redispersed in ethanol, where they were stored at a final concentration of 10 mg/ml. Prior to experiments the particles were centrifuged again and transferred into 10 ml of toluene. For the aqueous phase of the emulsion, 300 μl double distilled water was added to the toluene immediately before observation in the microscope. The emulsion was formed by gentle mixing with the pipette.

Silanized silica microspheres form a hexagonal lattice at the water oil interface already at relatively low areal densities compared to polystyrene beads – this can be attributed to long range interactions ¹¹. The lattice spacing of these dilute crystals is about five to seven times the particle diameter. Adsorption of additional particles at the oil-water-interface increases the areal density of the particles and a dense crystalline state is formed with a lattice spacing of about 1.2 particle diameters. At this stage the mobility of the particles is restricted. The crystalline structure is therefore quite stable over the very long scanning times (10 min) of the confocal imaging system (LSM510, Zeiss, Germany). The very high mobility of the particles during the formation of the crystal allows them to equilibrate. Images were taken with a 63x oil objective (numerical aperture 1.4) and the fluorescence excitation was achieved with a laser of 488nm and emission was observed with the help of a 505nm long pass filter.

Due to the different refractive indices of water ($n_w=1.33$) and toluene ($n_t=1.49$) the water drop acts like a downscaling lens: the hemisphere which is farther away from the microscope's objective appears to be smaller than the one closer to it. Oswald ripening of the emulsion was observable: larger crystals grow at the expense of smaller crystals. As all silanized silica beads remained on the surface, when shrinking smaller crystals were forced to dent. Thus irregularly buckled crystal structures were observable after several hours, which were not further analyzed.

For the analysis of the three dimensional arrangement of the particles the 3D position of each colloid has been determined by a correlation algorithm. A test bead - the correlation kernel - is compared with a region in the original 3D image and a correlation image is produced by

$$\text{Correlation}(\vec{R}) = N(\vec{R}) \sum_{\vec{r} \in \text{Kernel}} \text{Image}(\vec{R} + \vec{r}) \cdot \text{Kernel}(\vec{r})$$

where Correlation, Image and Kernel denote the 3D arrays containing the intensities of the three images respectively. \vec{R} and \vec{r} are vectors with three components and simply point to a pixel in one of the images. N is a normalization constant to suppress artifacts in the correlation image produced by large regions with overflow intensities set to 1 in order to save computation time. The correlation algorithm results in higher intensities the better the region around the corresponding pixel in the original image data resembles the kernel. The bead positions are thus determined by the local maxima in the correlation image. This procedure was quite successful and failed only in the equatorial region or regions with very low contrast. To check whether this method worked properly we marked the positions of the beads gained by the correlation back into the original image data and thus tracking artifacts could be corrected manually.

To eliminate the lens effect of the water drop we fitted a sphere to the bigger undistorted hemisphere. Then we shifted and scaled (with respect to the sphere's centre) the coordinates of all beads in the smaller half collectively so that deviation from the fitted sphere was minimized. This was necessary for a proper triangulation of the crystal. It also yielded the most accurate centre position of the crystal and its radius. The obtained bead positions were then used for the Delaunay tessellation. For a 2D flat lattice the Delaunay tessellation consists of all triangles whose circumcircles contain but the three vertices of

that triangle ¹². We adapted this to the spherical case and searched instead for triangles on the sphere's surface whose cones (defined by the circumcircle of the triangle and its apex in the centre of the sphere) enclose just the three vertices of a triangle. We used an incremental algorithm for the tessellation: we first assume a region of the crystal is already triangulated and then choose an edge which is contained in only one triangle so far. Consequently, this triangle lies at the margin of the region which has been triangulated and this particular edge is the border between a triangulated and a non- triangulated region. In the next step a vertex is searched in the set of all lattice sites so that the triangle formed by that vertex and the edge satisfies the condition from above. Add this triangle to the set of already found triangles and move on to the next edge. To find an initial edge around which the triangulation can grow one can pick for instance an arbitrary point and search for its nearest neighbor. For the implementation of all algorithms we chose MatLab. Dislocations which were separated by less than 2 lattice spacing were identified as scars.

The silanized silica beads assembled in crystalline structures as can be seen in Fig. 1. As aggregation of the colloidal particles in the oil phase could not be prevented completely, a few aggregates were always observable. Although some of these aggregates stuck to the spherical crystals or even sometimes were incorporated into the crystal structure, only local disturbances of the hexagonal lattice were observable. We choose to study only crystals with an approximate system size in the range of $R/a \sim 11$ to 14, where in the ground state already scars of a length of about 3 dislocations are expected to occur. In the shown crystal the mean lattice spacing a was $1.8\mu\text{m}$ and the radius of the crystal was found to be $22\mu\text{m}$. Most of the spherical surface was covered by a hexagonal lattice, as is apparent after triangulation of the crystal. Only in the equatorial area the optical resolution was not sufficient to determine the particle positions accurately. Thus a total triangulation of the solid angle 2π (50%) of the sphere was achieved. Apart from the most prominent scars only a few isolated dislocations were observable in the continuum hexagonal lattice. In the example shown 8 scars have been identified each containing between 3 and 6 excess dislocations with each scar possessing one excess 5-fold disclination. The total number of scars and their average length of 4 was thus in good accordance with the

theoretically expected lengths. Similar distributions of scar lengths was found for all analysed spherical crystals with system sizes R/a in the range of 11 to 14. The scars were highly curved as can be seen in Fig. 2.

Some of the straighter scars were used to analyse the nature of the grain boundary in greater detail. As can be seen in Fig. 3, the grain boundary angle of the crystal is continuously changing: from approximately 30° at the centre to vanishing at the end of the scar. This change of the angle results from the curvature of the surface: the further one is away from the centre of the scar the more the elastic distortion of the lattice is screened by the curvature of the sphere and the interior dislocations, resulting in less angular mismatch between the orientation of crystallographic axes on each side of the grain boundary. Eventually, the total disclination charge is effectively screened completely and the grain boundary freely terminates – a phenomenon that could not occur in flat space. The particular angles we observe are probably affected by thermal fluctuations of the grain boundary as well. The phenomenon is more regular at zero temperature.

To examine the alignment of the scars with respect to each other we calculated the angles between the scars. As reference point for each scar we chose the 5-fold coordinated bead in the middle of the scar. If each scar is centered at a vertex of an icosahedron as theory predicts, four different angles have to occur: 0° , 63.4° , 116.6° and 180° . Some of the observed angles were in good accordance with these but others were not. This can be visualized by fitting an icosahedron to the 5-fold coordinated bead in the middle of the scars (Fig. 4). As can be seen, some scars are located rather well on the vertices of an icosahedron while others are not. We also did not observe any clear trend in the relative orientation of the scars. Both findings can be attributed to the marked effect of thermal fluctuations in the system. The existence of clusters and aggregates adhering at some locations of the crystals' surface could also perturb the long range order, despite the fact that they are clearly not disturbing the short range order of the crystal. It is possible that the elastic interaction energy between different scars is influenced by these defects and thus they are not perfectly equilibrated. This would be in accordance with the finding that the location of scars on the hemisphere with no adhering clusters are close to the vertices of the

icosahedron, while on the hemisphere where some clusters were adhering the scars were not centered on the vertices of an icosahedron.

The system we studied here has allowed us for the first time to observe the static structure of scars on an entire spherical surface. In this way we demonstrate that the topological features of the sphere are indeed present in the ground state (12 clusters of defects in all). In contrast to the curved crystal systems previously studied the dislocations we observe here are not very mobile over the time scale of the experiment ¹³. Although the structural features are consistent with the broad predictions of equilibrium statistical mechanics there is most likely some kinetic trapping occurring. Nevertheless we confirm both the presence of the correct number of scars and the proper growth in their length as a function of system size. We observed that experimentally inevitable clusters and aggregates disturb the structure of the crystal only locally – however, the overall static structure of the lattice is not affected. Still, the icosahedral symmetry of the scars' alignment may have been disturbed by their presence. This demonstrates the intrinsic nature of the defect scars. One can speculate that melting in this system would be initiated at the grain boundary arrays and thus the presence of scars may be crucial in understanding phase transitions in spherical crystal structures.

Acknowledgements

This work was supported by the DFG (BA2029-5) and the Fonds der Chemischen Industrie. The work of MJB was supported by the National Science Foundation through Grant No. DMR-0219292 (ITR).

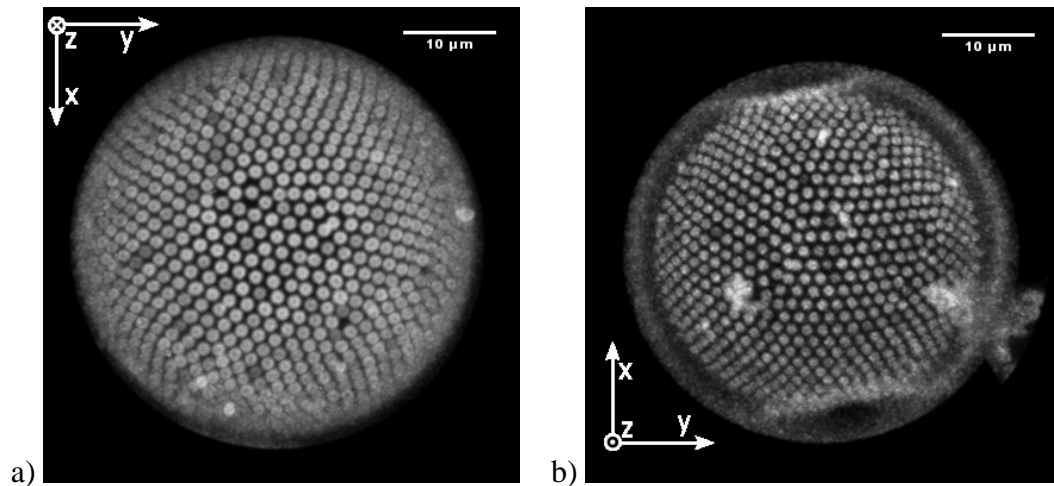


Fig.1: Projection of a confocal image of a spherical crystal ($R=22\text{ }\mu\text{m}$, $R/a = 12$). a) lower half of the crystal, the optical axis is pointing into the image b) upper half of the crystal as viewed from above, therefore the optical axis is pointing out of the image. Colloids which were not adsorbed at the interface are not shown in the image. Scale bar is $10\mu\text{m}$. The seemingly irregular shape of the crystal does not arise from the dents caused by Ostwald ripening, but rather from optical distortion caused by refraction of the light at adjacent water droplets which are not shown in the images.

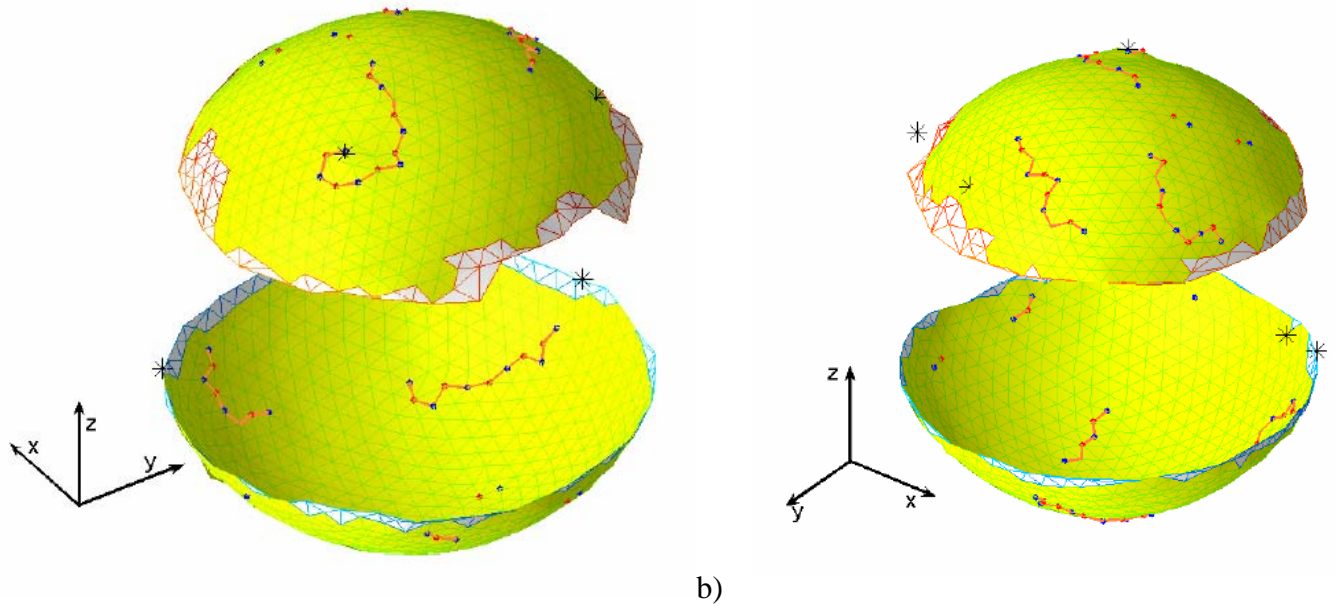


Fig. 2: a) Triangulated sphere shown in Fig. 1 ($R = 22\mu\text{m}$, $R/a = 12$, $N=2100$) b) Same sphere rotated around the optical axis by 180° . Blue and red marked lattice sites denote five fold and seven fold coordinated beads respectively. The asterisks indicate the positions of attached clusters which did not cause local disturbances of the lattice symmetry. The observed scars consist of 3 to 6 dislocations and one excess five fold disclination. Scars which are too close to the equatorial region cannot be analyzed. Some free, probably thermally excited, isolated dislocations are also visible. Shown coordinate axes are $10\mu\text{m}$.

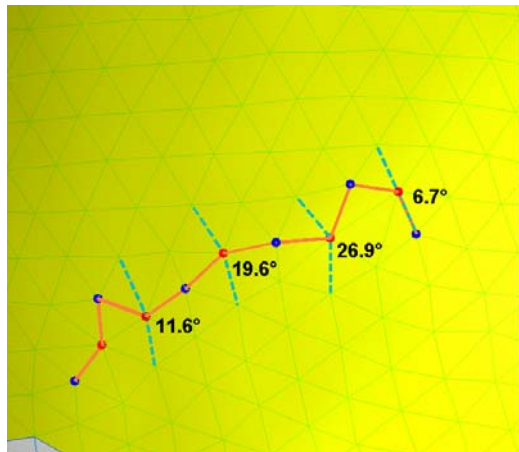
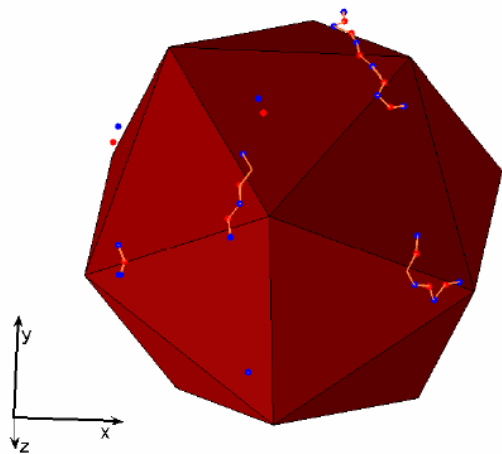


Fig. 3: The grain boundary angle varies along the scar shown is a zoom in into the scar located on the right side on the lower half of the crystal shown in Fig. 2 a.

a)



b)

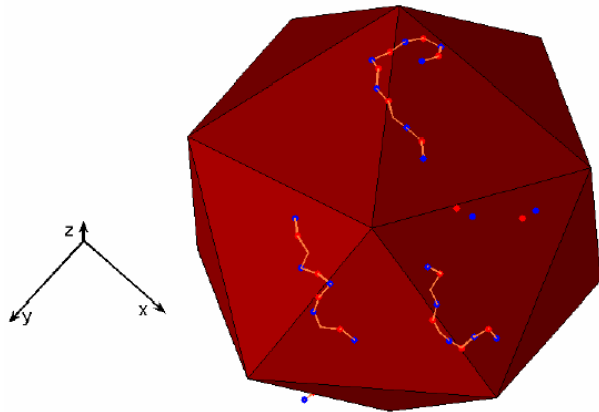


Fig. 4: Alignment of the scars. The experimentally determined scars were plotted and an icosahedron was oriented so that the scars' positions fit best to the vertices of the polyhedron. Viewpoints in a) and b) are similar to the projections shown in Fig. 1. Note that the scars do not lie exactly on the vertices. Especially in the upper half shown in b) deviations of the ideal icosahedral symmetry is observed. In this half 3 colloidal clusters were adhering to the crystal. Deviations can mainly be explained by thermal excitation of the crystal or local disturbances by adhering clusters. Shown coordinate axes are 10 μ m.

- (1) Bowick, M. J.; Nelson, D. R.; Travesset, A., *Phys. Rev. B: Condens. Matter* **2000**, 62, 8738.
- (2) Schneider, S.; Gompper, G., *Europhys. Lett.* **2005**, 70, 136.
- (3) Vitelli, V.; Turner, A. M., *Phys. Rev. Lett.* **2004**, 93.
- (4) Travesset, A., *Physical Review B* **2003**, 68.
- (5) Bowick, M.; Cacciuto, A.; Nelson, D. R.; Travesset, A., *Phys. Rev. Lett.* **2002**, 89.
- (6) Bausch, A. R.; Bowick, M. J.; Cacciuto, A.; Dinsmore, A. D.; Hsu, M. F.; Nelson, D. R.; Nikolaides, M. G.; Travesset, A.; Weitz, D. A., *Science* **2003**, 299, 1716.
- (7) Pickering, S. U., *J. Chem. Soc. Trans.* **1907**, 91, 307
- (8) Binks, B. P., *Curr. Opin. Col. & Int.* **2002**, 7, 21.
- (9) Binks, B. P.; Lumsdon, S. O., *Phys. Chem. Chem. Phys.* **1999**, 1, 3007.

- (10) Binks, B. P.; Lumsdon, S. O., *Langmuir* **2000**, 16, 8622.
- (11) Horozov, T. S.; Aveyard, R.; Clint, J. H.; Binks, B. P., *Langmuir* **2003**, 19, 2822.
- (12) Delaunay, B., *Bull. Acad. Sci. USSR* **1934**, 7, 793
- (13) Lipowsky, P.; Bowick, M. J.; Meinke, J. H.; Nelson, D. R.; Bausch, A. R., *Nature Mat.* **2005**, 4, 407.